

The Use of Nanoparticles to Deliver Nitric Oxide to Hepatic Stellate Cells for Treating Liver Fibrosis and Portal Hypertension

Hien T. T. Duong, Zhixia Dong, Lin Su, Cyrille Boyer, Jacob George, Thomas P. Davis,* and Jianhua Wang*

Polymeric nanoparticles are designed to transport and deliver nitric oxide (NO) into hepatic stellate cells (HSCs) for the potential treatment of both liver fibrosis and portal hypertension. The nanoparticles, incorporating NO donor molecules (S-nitrosoglutathione compound), are designed for liver delivery, minimizing systemic delivery of NO. The nanoparticles are decorated with vitamin A to specifically target HSCs. We demonstrate, using *in vitro* and *in vivo* experiments, that the targeted nanoparticles are taken up specifically by rat primary HSCs and the human HSC cell line accumulating in the liver. When nanoparticles, coated with vitamin A, release NO in liver cells, we find inhibition of collagen I and α -smooth muscle actin (α -SMA), fibrogenic genes associated with activated HSCs expression in primary rat liver and human activated HSCs without any obvious cytotoxic effects. Finally, NO-releasing nanoparticles targeted with vitamin A not only attenuate endothelin-1 (ET-1) which elicits HSC contraction but also acutely alleviates haemodynamic disorders in bile duct-ligated-induced portal hypertension evidenced by decreasing portal pressure ($\approx 20\%$) and unchanging mean arterial pressure. This study clearly shows, for the first time, the potential for HSC targeted nanoparticle delivery of NO as a treatment for liver diseases with proven efficacy for alleviating both liver fibrosis and portal hypertension.

1. Introduction

Liver fibrosis and its end-stage cirrhosis, result from chronic liver injury. At present, the curative treatment for end stage liver cirrhosis with high survival rate is liver transplantation.

However, the limited supply and increasing demand for donor livers as well as the issues of compatibility with the recipient's liver are the major challenges for liver transplantation. There is therefore a critical and unmet need to develop anti-fibrotic strategies to treat liver disease.

Dr. H. T. T. Duong, Prof. C. Boyer
Australian Centre for Nanomedicine and Centre for
Advanced Macromolecular Design
School of Chemical Engineering
University of New South Wales
Sydney 2052, Australia

Dr. Z. Dong, Dr. L. Su, Prof. J. George, Dr. J. Wang
Storr Liver Unit
Westmead Millenium Institute
and Westmead Hospital
University of Sydney
Sydney, NSW, Australia
E-mail: jianhua.wang@sydney.edu.au

DOI: 10.1002/sml.201402870

Dr. Z. Dong
Shanghai First People's hospital
School of Medicine
Shanghai Jiaotong University
China

Prof. T. P. Davis
ARC Centre of Excellence in Convergent Bio-Nano Science & Technology
Monash Institute of Pharmaceutical Sciences
Monash University
Parkville, Melbourne, VIC 3052, Australia
E-mail: thomas.p.davis@monash.edu

Prof. T. P. Davis
Department of Chemistry
University of Warwick
Coventry, UK



In 1992, nitric oxide (NO) was named as “Molecule of the Year” by *Science* because of broad-spectrum biological effects.^[1] NO is an important cellular signaling molecule and a deficiency of NO has been associated with many medical problems such as diabetes,^[2] liver fibrosis,^[3] cardiovascular illness,^[4] neurodegenerative diseases,^[5] and several cancers.^[6] However, a major problem using systemic delivery of NO as a therapeutic molecule is its high indiscriminate reactivity and its influence in many biological functions, restricting the development and fabrication of a targeted delivery system for effective NO delivery.

In vitro and in vivo studies have demonstrated that exposure to gaseous NO can result in the down regulation of profibrogenic mediators such as collagen and TGF beta 1, thus attenuating liver fibrosis.^[7] In addition, NO supplementation can improve portal hypertension, which is one of the life threatening complications of liver cirrhosis, by reducing intrahepatic resistance. Hepatic stellate cells (HSCs) play a central role in the development of fibrosis and portal hypertension following injury/damage because they secrete and accumulate extracellular matrix (ECM) in the liver.^[8] In healthy liver cells, HSCs are non-parenchymal, quiescent cells with the main function of storing vitamin A, probably to maintain normal ECM levels by mediating ECM turnover.^[8] Once activated (following liver injury), HSCs go through a phenotypic transformation and acquire myofibroblast-like features characterised by a loss of vitamin A, high rates of proliferation, increased production of collagen, growth factors and cytokines and increased cell contractility resulting in a significant influence on sinusoidal blood flow.^[9] The contraction of HSCs in fibrotic livers causes a significant increase in portal venous pressure that is termed portal hypertension. Therefore, studies on therapeutic agents to inhibit the activation and proliferation of HSCs, reduce HSC-ECM production and inhibit HSC contraction, could lead to beneficial approaches for the treatment of liver fibrosis/cirrhosis and portal hypertension.

Although the understanding of the role of NO in suppression of liver fibrosis is still unclear, many recent published evidence has demonstrated that administering nitric oxide to cirrhotic rats down regulates the expression of collagen I, α -smooth muscle actin (α -SMA) and platelet-derived growth factor (PDGF).^[10] In vitro experiments demonstrated that NO exposure can inhibit HSC proliferation and migration, promote HSC apoptosis, down-regulate the activation marker α -SMA and suppress collagen I gene expression.^[11] Thus, prior evidence suggests that NO exposure can exert beneficial therapeutic effects in mediating liver fibrosis when administered to HSCs.

The in vivo delivery of NO is challenging and systemic administration is unlikely to be an option for the treatment of end stage liver disease. The exogenous delivery of NO to organs other than the lungs in a controlled manner is incredibly challenging, as NO gas has limited solubility in water (2×10^{-3} to 3×10^{-3} M) and NO is an extremely reactive molecule that can react with oxygen (and other gases) resulting in a short half-life time in the body (0.1–5 s).^[12] To improve the administration of NO gas, a range of small donor molecules have been developed, capable of decomposition under

specific conditions. An ideal NO donor would (i) be stable for an extended period of time, (ii) nontoxic and noninflammatory, and (iii) release NO at the pharmacologically specified dose and time.^[12b]

Among the NO donors, S-nitrosothiols (RSNOs) and N-diazoniumdiolates (NONOates) are the most widely used for NO delivery. Unfortunately, small molecule, NO-donors lack both stability and specificity; e.g., NONOate compounds, such as, spermine NONOate, have a half-life of only a few minutes at 25 °C in water. Nonspecific and systemic administration of NO can result in serious side effects, such as hypotension, therefore any NO donor would need to be targeted to the specific disease site before being activated to release NO. Here this limitation has been overcome by encapsulating NO donors in polymer nanoparticles to enhance the biological stability of NO, and to attach biorecognition molecules for cell specific targeting.^[13] In our previous work,^[13a] we demonstrated the encapsulation of NO donors in polymeric nanoparticles, significantly extending the half-life of NO donors. In this work, we demonstrate, for the first time, that polymeric nanoparticles decorated with vitamin A can be employed as nanocontainer for the specific and controlled delivery of NO to the HSCs of the liver in vivo and in vitro. In addition, we demonstrate that vitamin A can be employed to target specifically HSCs. The rationale for using vitamin A is that HSCs absorb and store $\approx 80\%$ of retinols in the body.^[14] Recently, Sato et al.^[15] reported that vitamin A loaded liposomes (approximate size 150 nm) could interact with RBPs through RBP receptors on HSCs to deliver siRNA for gene silencing. In this article, we show, for the first time, that vitamin A decorated polymeric nanoparticles are an efficient nanocarrier for the treatment in liver fibrosis by inhibiting the collagen production and reducing concomitant portal hypertension, which is one of the severe complications of liver fibrosis.

2. Results and Discussion

2.1. Design of NO-Polymeric Nanoparticles Decorated Without and With Vitamin A

The synthesis of NO-polymeric nanoparticles without vitamin A was reported in our previous publication.^[13a] Briefly, we prepared diblock copolymers (POEGMA-*b*-VDM) via reversible addition fragmentation chain transfer polymerization.^[16] First, oligoethylene glycol-methacrylate (OEGMA) was polymerized in the presence of (4-cyanopentanoic acid)-4-dithiobenzoate as a chain transfer agent and 2,2'-azobisisobutyronitrile (AIBN) as initiator. After purification, the polymers were chain extended with 2-vinyl-4,4-dimethyl-5-oxazolone monomer (VDM) yielding diblock copolymers (**Figure 1A**). ¹H NMR, FTIR spectroscopy, and GPC confirmed the VDM incorporation (Figures S1–S4, Supporting Information). ¹H NMR was employed to assess the composition of VDM in the polymers (Table S1, Supporting Information). Azlactone groups were subsequently used to attach S-nitrosoglutathione (GSNO) to the polymeric chains. The amino group of GSNO was conjugated to the

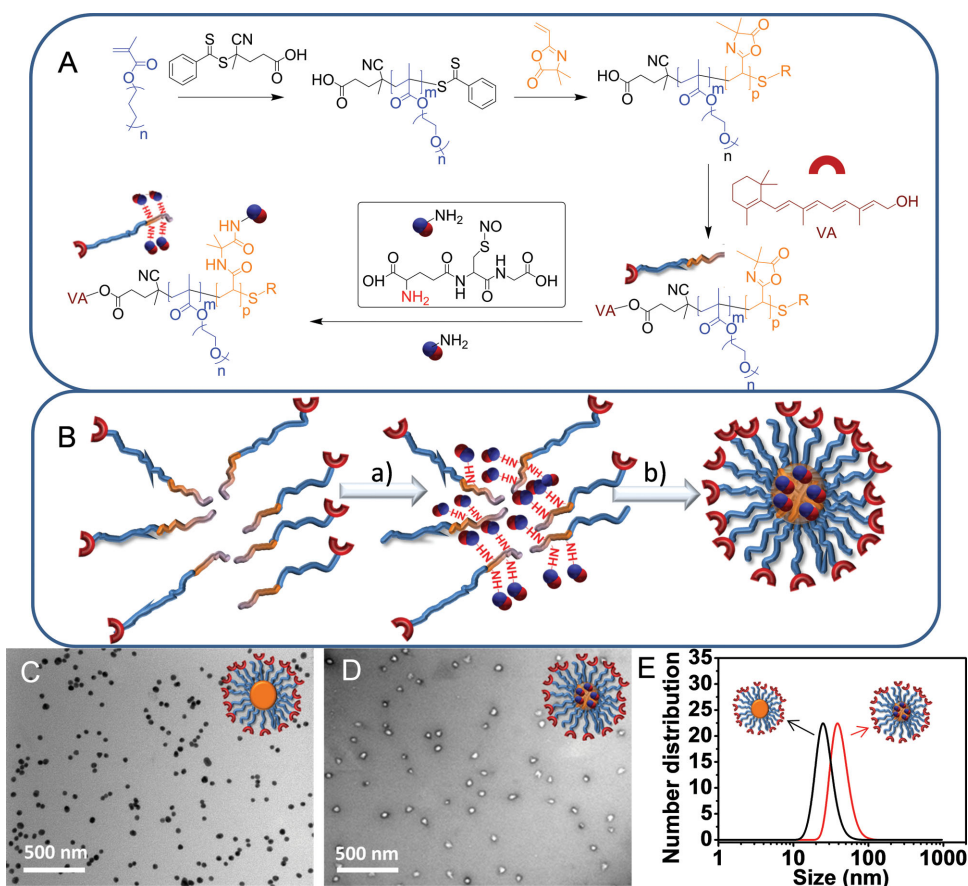


Figure 1. A) Description of the synthetic approach employed to synthesize vitamin A coupled nanoparticles loaded with S-nitrosoglutathione (GSNO). B) Schematic representation of the synthesis: a) POEGMA-*b*-VDM was reacted with GSNO in DMSO and b) the purified GSNO-copolymers were added in water to yield polymeric nanoparticles; TEM images of vitamin A coupled nanoparticles C) without NO donors; D) with NO donors (high magnification images are included in the Supporting Information). E) Dynamic light scattering of the vitamin A coupled nanoparticles with and without NO donors.

azlactone in dimethyl sulfoxide (DMSO) and the successful attachment of GSNO was confirmed using NMR, FTIR, and UV-vis spectroscopy (Figures S3–S6, Supporting Information) in good accord with our previous publications.^[13a] The nanoparticles were formed by slow addition of water in DMSO with GSNO conjugated polymer. After purification by using dialysis against water and freeze-drying, about 10% of azlactone groups was remained according to NMR and FTIR at 1820 cm^{-1} . The azlactone groups were intentionally left unreacted to maintain the hydrophobicity in the core of the nanoparticles. Finally, UV-vis spectroscopy was invoked to determine the amount of GSNO conjugated to the polymers using the characteristic signal of S-NO at 544 nm and the following equation: $[\text{GSNO}] = (\text{Abs}^{544}/(\epsilon^{544} \times l)) \times 100$, with Abs^{544} , l and ϵ^{544} correspond to the absorbance at 544 nm, path length of 1 cm and extinction coefficient of GSNO ($15.0\text{ M}^{-1}\text{ cm}^{-1}$).^[17]

For the synthesis of polymeric nanoparticles decorated with vitamin A, the carboxylic acid end-groups of the chain transfer agent were exploited to conjugate retinol (vitamin A) via a simple esterification reaction in DMSO using DCC and DMAP as catalysts. Because vitamin A is light sensitive, the coupling reaction was protected from light. After purification, vitamin A attachment and the amount of vitamin A

attached to the polymer was determined by UV-vis using the absorbance at 328 nm (Figure S7, Supporting Information). Vitamin A solution in DMSO at different concentrations were carefully prepared to achieve the absorbance reading between 0.1 and 1.0 units at 328 nm. The amount of vitamin A conjugated in the polymer was 0.43% (by weight) which corresponded to 0.52 mol vitamin A per mol of polymer.

Transmission electron microscopy (TEM) (Figure 1C,D, and Figure S8, Supporting Information) and dynamic light scattering (DLS, Figure 1E) were employed to determine the size of the nanoparticles with vitamin A before conjugation with GSNO, showing a size of around 25 nm. After conjugation with GSNO, TEM micrographs indicated an increase in size (35 nm). It is interesting to note, that after conjugation of GSNO to the polymeric nanoparticles, interaction with the electron beam during the TEM analysis caused NO release, resulting in the formation of hollow nanoparticles (Figure 1D and Figure S8, Supporting Information). It is noted that there is only a slight change in the size of the nanoparticles (with and without GSNO) after conjugation with vitamin A.

One of the major drawbacks of GSNO compounds, as NO donors, is their poor stability in aqueous solution. GSNO has a half-life of few days at room temperature, limiting its storage. In the meanwhile, the stability of GSNO

encapsulated in nanoparticles was improved for several days.^[13a] In this present study, we confirmed that the presence of vitamin A on the nanoparticle surface did not change the stability of encapsulated GSNO (data not shown). The stability tests were performed using UV visible spectroscopy, monitoring the absorbance bands at 544 nm following both the release of NO from free GSNO and GSNO encapsulated in the polymeric nanoparticles, as shown in Figure S6, Supporting Information.

The release of NO from S-nitrosothiol compounds can be induced by different stimuli such as light, pH or redox chemistry. A convenient mechanism for intracellular NO release from donor molecules, is the reaction with a reducing agent such as glutathione, ascorbic acid or with metallic ions such as copper. We exposed the NO-loaded nanoparticles decorated by vitamin A to ascorbic acid (5.0×10^{-3} M) to mimic the cellular environment (cytosol) and the release of NO was monitored by UV-vis spectroscopy via the decrease of the absorption peak at 544 nm. GSNO was also tested under similar conditions. The NO time-release profiles from both GSNO and GSNO-nanoparticles decorated vitamin A are similar to reported data in our previous paper (data not shown).^[13a] In the presence of ascorbic acid (reducing agent), over 80% of NO was released from the nanoparticles after 24 h. The expected NO release mechanism was confirmed using Raman spectroscopy, verifying the formation of disulfide bonds following NO release, with the appearance of an absorbance peak at 500 nm consistent with earlier reports^[13a,18] (Figure S9, Supporting Information).

2.2. In Vitro HSC Targeting of Vitamin A Conjugated Nanoparticles

In addition to their key role in the onset of fibrosis, HSCs actively take up and store vitamin A via receptors for retinol binding protein (RBP). The specific uptake of vitamin A decorated nanoparticles by HSCs was investigated using fluorescent nanoparticles loaded with Nile Red. As a control, we prepared vitamin A free nanoparticles also loaded with Nile Red. The presence of Nile Red in the nanoparticles was confirmed by UV-vis spectroscopy via the absorption at 450 nm. DLS data showed size of nanoparticles of around 30 nm after encapsulating with Nile Red. Flow cytometry was then used to measure the uptake of both of these nanoparticles in primary rat hepatic stellate cells and human hepatic cells (LX-2). The control nanoparticles exhibited poor uptake as indicated by low fluorescence intensities. In contrast, vitamin A decorated nanoparticles accumulated rapidly in both rat hepatic stellate cells and LX-2 cells. Maximum nanoparticle accumulation was observed after 30 min of incubation as indicated by an order of magnitude increase in fluorescence intensity (Figure 2 and Figure S11, Supporting Information). An enhanced specific uptake of vitamin A-coupled nanoparticles by HSCs via the RBP receptor was also confirmed by significant increases ($\approx 30\%$.) in fluorescence intensities in flow cytometry measurements when vitamin A-coupled nanoparticles were incubated with rat HS cells in the presence of RBP.

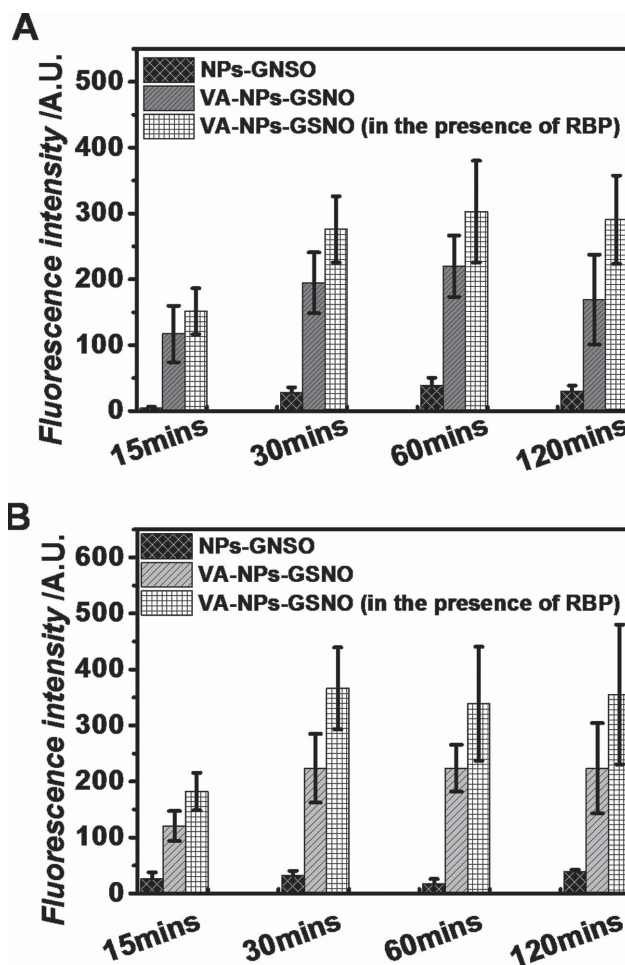


Figure 2. Cell uptake of nanoparticles labeled with Nile Red expressed as mean fluorescence intensity using A) rat primary HSCs at day 6 and B) human LX-2 cell line. Results are means \pm SD of at least three independent experiments performed in triplicate.

The results from flow cytometry were reinforced by fluorescence microscopy measurements. As shown in Figure 3C, after 6 h, rat HSCs incubated with vitamin A-coupled nanoparticles (labeled with Nile Red) showed much higher accumulation in the cytoplasm when compared to vitamin A free nanoparticles (Figure 3B). The uptake of rat HSCs with vitamin A-coupled nanoparticles was enhanced in the presence of RBP (Figure 3D). A similar result was obtained for human HSCs (LX-2) (data not shown).

2.3. In Vivo Biodistribution of Vitamin A Decorated Nanoparticles

To assess the feasibility and suitability of a nanoparticle drug delivery system for liver fibrosis treatment, it is vital that the nanoparticles preferentially accumulate in the liver and in the HSCs in vivo. The biodistribution of vitamin A decorated nanoparticles (labeled with Nile Red) was investigated post-humously in normal and bile duct-ligated (BDL) rats using fluorescence visualization of liver, kidney, eye, heart, spleen, brain, intestine, and lung tissue homogenates 2 h after tail vein injection. It is well known that the biodistribution and

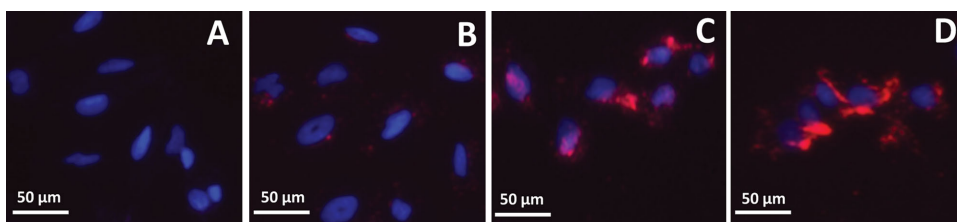


Figure 3. Fluorescence microscopy of rat HSCs incubated for 6 h with polymeric nanoparticles. A) Untreated cells (control), B) vitamin A free, Nile Red labeled nanoparticles, C) vitamin A-coupled, Nile Red labeled nanoparticles, D) vitamin A-coupled, Nile Red labeled nanoparticles in the presence of RBPs. Note: Nile Red concentration is equivalent to 100 $\mu\text{g}/\text{ml}$, nuclei were stained with DAPI. Nile Red fluorescent images were acquired at $\lambda^{\text{ex}} = 488 \text{ nm}$ and $\lambda^{\text{em}} = 595 \text{ nm}$.

clearance rate of nanoparticles after intravenous injection are influenced by many factors including the physicochemical properties of nanoparticles (size, shape, chemistry surface, and charge) and physiological conditions.^[19] To obtain a longer residence time in the body, we decided to functionalize the nanoparticles with a POEGMA segment (structurally similar to PEG), as it is known that PEG can increase the blood half-life of nanoparticles, reducing clearance by the reticuloendothelial system (RES).^[20] After administration, nanoparticles rapidly accumulated in the livers of both normal and BDL rats (**Figure 4**). Interestingly, the liver accumulation was higher for BDL rats when compared to normal rats, a result which can be explained by the larger number of HSCs following proliferation during the activation process. We observed some fluorescence in the kidneys. We hypothesized that this observation may indicate an elimination pathway (alternatively—or additionally, the kidney has mesangial cells that may also attract vitamin A targeting). Due to their vasculature and fenestrae, it is expected the higher accumulation of nanoparticles presented in some organs such as liver, kidney, lung, spleen than other organs. This can actually be an advantage for using the polymeric nanoparticles in this study for the targeted delivery of nitric oxide to the hepatic stellate cells in the liver. It is also well-documented in the literature that renal failure (also known as kidney failure) is one of the severe complications in the patients with liver cirrhosis.^[21] This type of renal dysfunction is known as

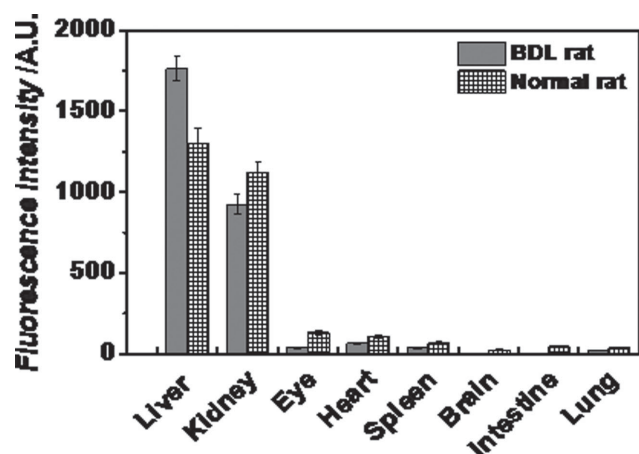


Figure 4. Biodistribution in different organs of vitamin-A decorated nanoparticles (labeled with Nile Red) in normal and BDL rats after 2 h post-injection. Results are means \pm SD of three independent experiments. Note: A.U. stands for arbitrary unit.

hepatorenal syndrome (HRS), which is the unique form of failure in patients with liver cirrhosis, liver failure, and portal hypertension. The mechanism for HRS is complex, however the vasoconstriction is believed to influence on the renal circulation.^[21] Clinically, the solution for this complication is the use of vasodilator (mainly nitric oxide) in order to improve the renal circulation. The increase in NO production by enhanced eNOS activity was demonstrated to provide a protective role in the development of renal tissue injury by minimizing oxidative stress.^[22] Therefore, the accumulation of our nanoparticles in the kidney could be an advantage to overcome the HRS syndrome in patients with liver cirrhosis. Very low levels of nanoparticles were detected in the eye, heart, and spleen and only negligible traces were observed in the brain, intestine, or lungs.

Subsequently, we monitored the biodistribution over a longer period for vitamin A coupled nanoparticles labeled with Cy7.5 encapsulated in the core using noninvasive *in vivo* imaging analysis at different time points following intravenous injection through the tail vein. After injection, the accumulation of nanoparticles in different organs could be easily visualized by fluorescence emission. After 15 min post-injection, intense fluorescence was observed only in the liver but not in any other organs, confirming accumulation of vitamin A coupled nanoparticles in the liver. The fluorescence intensity remained relatively unchanged up to 48 h, with a gradual reduction at 96 h, completely disappearing at 120 h (**Figure 5**). *In vivo* imaging revealed that the PEGylated nanoparticles with vitamin A on the surface exhibited long accumulation in liver (around 2 days) avoiding fast excretion by macrophage cells. This result is consistent with previous published studies using PEGylated nanoparticles.^[23]

After confirming (almost exclusive) liver-accumulation following systemic administration, our second goal was to target HSCs (the cells causing the progression of liver fibrosis). In this experiment, all the primary cells were isolated and cultured for 6 days (for hepatic stellate cells), 2 days (for SECs, KCs and hepatocytes) following our well-established protocol with the purity of 95%.^[24] The cell uptake of nanoparticles labeled with Nile Red, by each cell line, was investigated as a function of incubation time at predetermined time points (15, 30, 60, and 120 min). HSCs were cultured for 6 days, as they undergo cell differentiation around 6 days. In contrast, KCs can be activated then have minimal phenotype change after few days. SECs can only survive for 3–4 days *in vitro* culture, thus these cells were cultured for 2 days in this experiment. Flow cytometry was performed to analyse

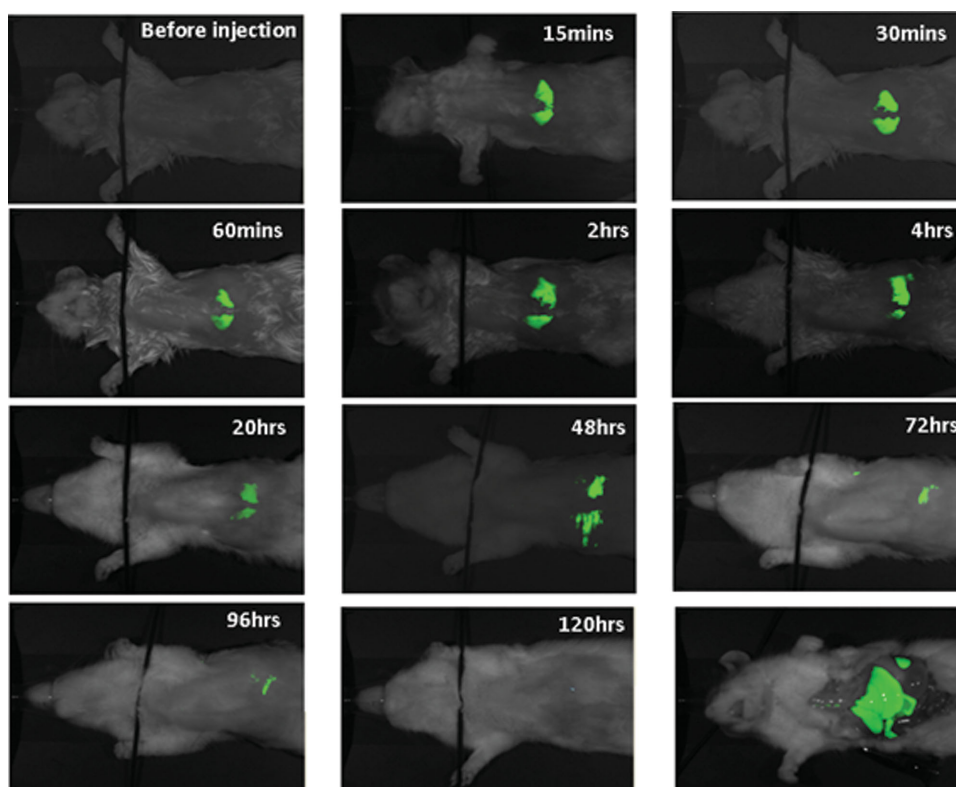


Figure 5. NIR images of BDL rats after intravenous injection of vitamin A coupled nanoparticles (labeled Cy7.5 NIR fluorescent dye). (Bottom right corner) bio-dissection of rat treated with vitamin A coupled nanoparticles (labeled Cy7.5 NIR fluorescent dye) after 4 h. Note NIR images taken by Pearl@Impulse small animal imaging system. Cy7.5 fluorescent images were acquired at $\lambda^{ex} = 788 \text{ nm}$ and $\lambda^{em} = 808 \text{ nm}$.

the uptake of vitamin A decorated nanoparticles labeled with Nile Red in HSCs, Kupffer cells and hepatocytes. As shown in Figure 6, the HSC uptake of vitamin A conjugated nanoparticles is significantly higher than for Kupffer cells (KCs), sinusoidal liver endothelial cells (SECs) or hepatocytes. As a control experiment, the accumulation of vitamin A free nanoparticles in HSC was found to be negligible (data not

shown). From the in vitro and in vivo data, it is evident that liver accumulation and HSC uptake are strongly favoured for vitamin A decorated nanoparticles, largely avoiding delivery to other cell types in the liver, including hepatocytes.

2.4. Cell Viability and Anti-Fibrogenic Effect of Free GSNO in HSCs

The activation and proliferation of HSCs are the key factors affecting the secretion of collagen and other extracellular matrix proteins such as α -smooth muscle actin (α -SMA), tissue inhibitors of matrix metalloproteinase (TIMP-1), ultimately leading to liver fibrosis. Therefore, inhibition of activated HSCs (or inhibition of collagen production) is an important therapeutic approach to liver fibrosis. Recent studies have indicated that NO inhibits the production of collagen and other extracellular matrix proteins from HSCs.^[7] We initially investigated the anti-fibrogenic effect of free GSNO on cultured rat HSCs at different concentrations ranging from 10×10^{-6} to $1000 \times 10^{-6} \text{ M}$ (Figure 7). The HSCs treated with free GSNO showed a dose-dependent decrease in mRNA levels of collagen type 1, α -SMA, and CTGF in comparison to control cells. In contrast, no significant differences were observed for TIMP1 or TGF beta1, indicating that not all profibrogenic activity was down-regulated (Figure 7A).

The activation of HSCs leads to a trans-differentiation to myofibroblasts that demonstrate increased proliferation,

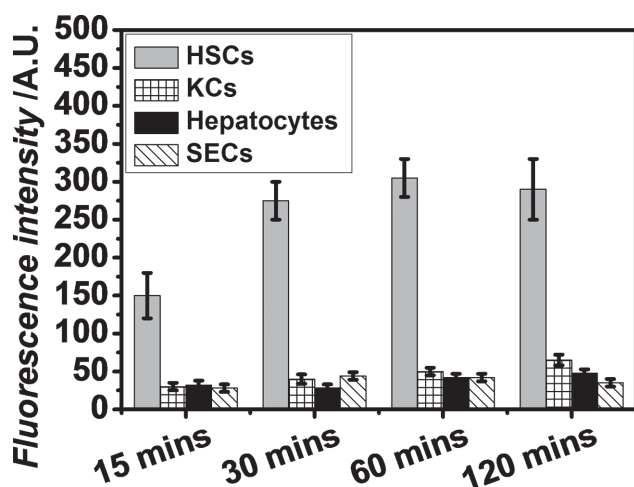


Figure 6. Cell uptake of vitamin A coupled nanoparticles (labeled Nile Red) in different rat primary cells at specified time points. Results are means \pm SD of at least three independent experiments performed in triplicate.

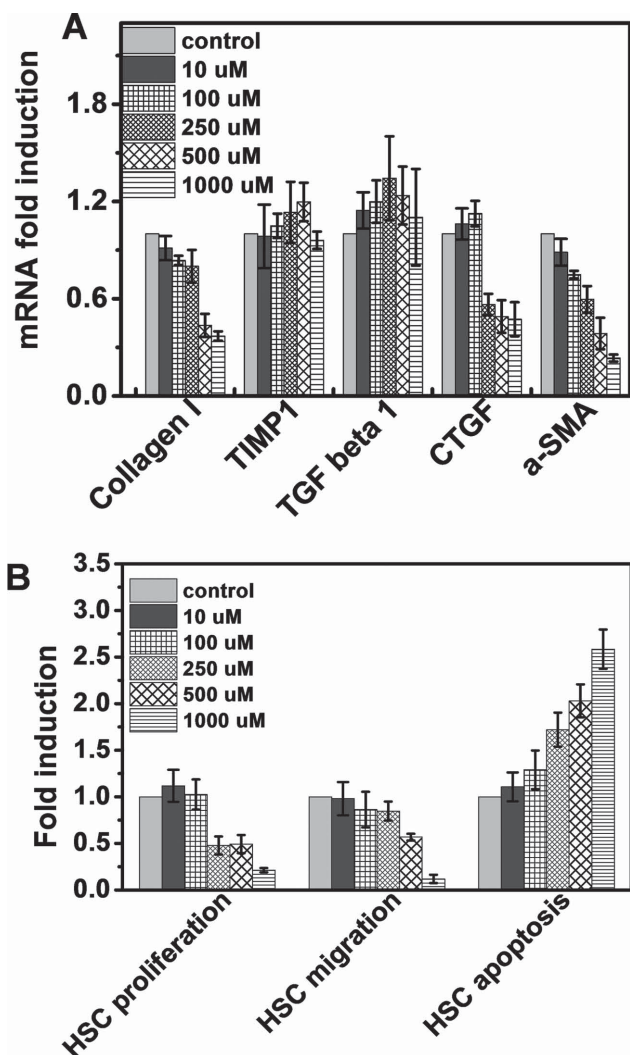


Figure 7. A) Expression of proliferation, apoptosis and migration of rat HSCs after treatment with GSNO. B) Expression of mRNA after treatment of rat HSCs with GSNO. Results are means \pm SD of at least three independent experiments performed in triplicate.

migration, contraction, and the production of ECM. As shown in Figure 7B, GSNO significantly inhibits the proliferation and migration of activated HSC/myofibroblasts in a dose-dependent manner. The inhibition of proliferation and migration of activated HSCs induced apoptosis of myofibroblastic HSCs.^[25] Cell viability studies on primary HSCs and human hepatic stellate cells LX-2 (after 72 h using Alamar Blue assay) demonstrated the nontoxic property of free GSNO at dose concentrations of between 10×10^{-6} and 500×10^{-6} M. Free GSNO starts showing cellular toxicity at concentrations above 500×10^{-6} M (Figure S10, Supporting Information).

2.5. Intracellular NO Release from NO-Nanoparticles in LX-2 Cells

Following confirmation that nanoparticles can release NO in vitro, we decided to investigate intracellular NO release using

4-amino-5-methylamino-2',7'-difluorofluorescein diacetate (DAF-FM DA) (Scheme S2, Supporting Information), which gives qualitative information. Indeed, quantitative measurements of NO in the cells and biologic media are extremely difficult due to the lack of stability of NO in these media.^[26] When DAF-FM DA reacts with NO, it emits a green fluorescence.^[27] LX-2 cells were incubated with the DAF-FM DA probe and then treated with VA coupled NO-nanoparticles. After 10 min, green fluorescence was observed, confirming the release of NO in the cells (Figure 8C). A control experiment was carried out in the absence of NO-nanoparticles, but in the presence of DAF-FM DA. A very weak fluorescence signal can be observed for the cells treated only with the probe (Figure 8B). Cells without any treatment (DAF-FM or NO-nanoparticles) did not yield any green fluorescence as expected (Figure 8A).

2.6. Vitamin A Decorated GSNO Nanoparticles Inhibits HSC Activated Phenotype In Vitro

We have investigated the anti-fibrogenic effect of free GSNO on cultured rat HSCs and the human LX-2 cell line. As shown in Figure 7, incubation with free GSNO at the concentrations of 250×10^{-6} , 500×10^{-6} , and 1000×10^{-6} M caused a significant down-regulation of pro-fibrogenic mRNA expression and inhibition of the activated phenotype (proliferation, migration, and apoptosis) on both cell types. Using Alamar Blue assays, we confirmed that GSNO at the concentration of 1000×10^{-6} M showed cellular toxicity on rat HSCs and the human LX-2 cell line. Thus 500×10^{-6} M GSNO was chosen to be an optimal dose for all of the following experiments. Non-functional nanoparticles, vitamin A decorated nanoparticles and vitamin A decorated nanoparticles with RBP were then incubated with rat primary HSCs (Figure 9A) and the human LX-2 cell line (Figure 9B). The expressions of messenger RNAs for collagen I, TIMP1, TGF beta, CTGF, and α -SMA were measured after nanoparticle treatment. The nanoparticles without vitamin A on the surface have been normalized to 1, and compared to the nanoparticles with vitamin A and vitamin A in the presence of RBP. In both cell lines, the nanoparticles with vitamin A on the surface induced significant decreases in collagen I, CTGF and α -SMA production of 60%, 40%, and 40%, respectively. As a control experiment, vitamin A decorated nanoparticles without GSNO were incubated with HSCs and the human LX-2 cell line. These nanoparticles did not change the production of collagen I, CTGF, and α -SMA production (data not shown). Also, nanoparticles with vitamin A on the surface inhibit the proliferation and

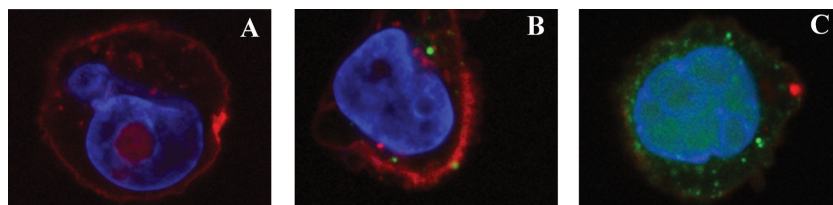


Figure 8. Confocal microscopy images of A) untreated LX-2 cells (control); B) treated LX-2 cells with DAF-FM; and C) treated LX-2 cells with DAF-FM and VA coupled NO-nanoparticles.

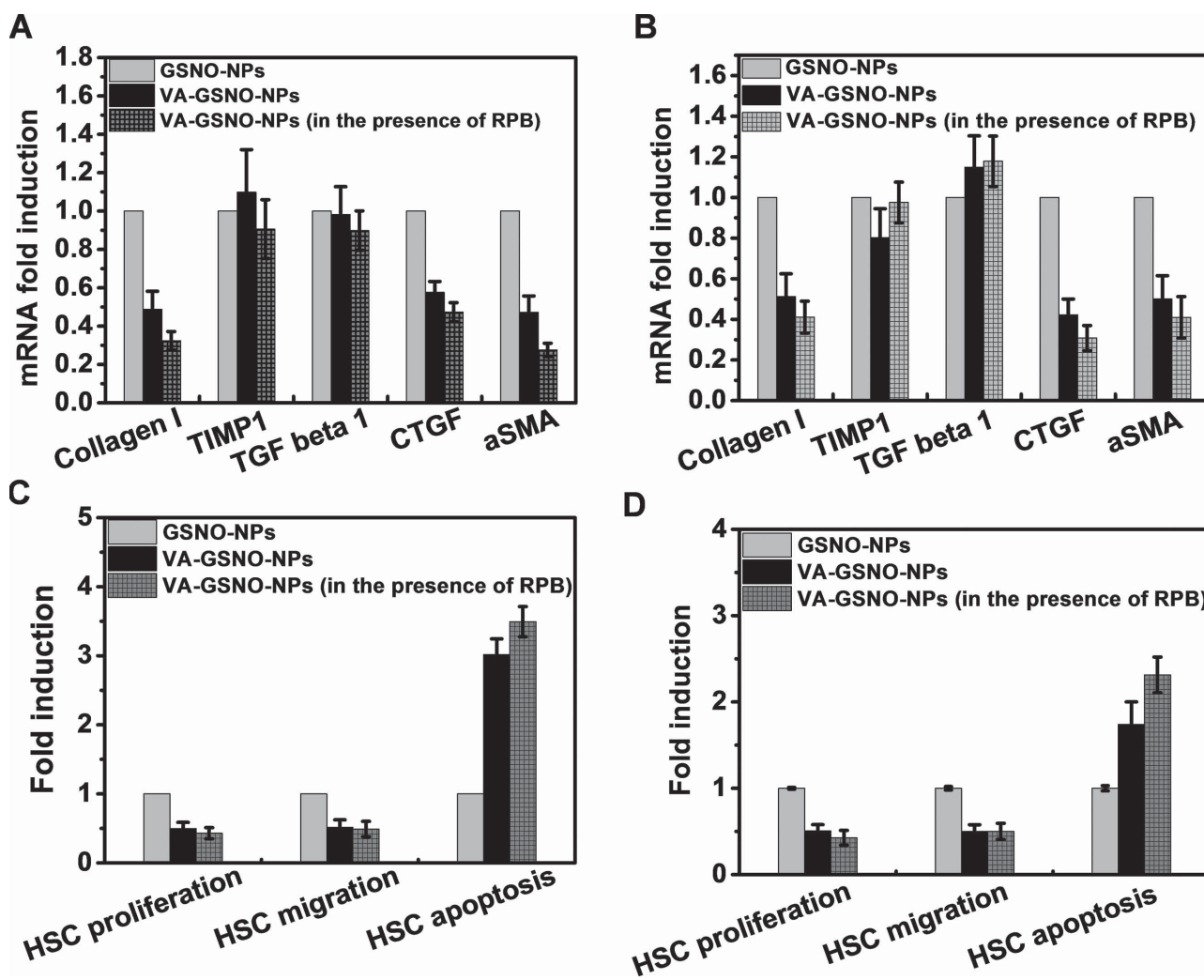


Figure 9. Expression of mRNA for different parameters in A) rat primary HSCs at day 6 and B) LX-2 cell line after treatment with GSNO nanoparticles. Expression of HSC proliferation, apoptosis and migration using C) rat primary HSCs and D) LX-2 cells. Results are means \pm SD of at least three independent experiments performed in triplicate.

migration which can induce the apoptosis of myofibroblastic HSCs (Figure 9C,D).

2.7. Effect of Vitamin A Conjugated NO Nanoparticles on Portal Hypertension

Portal hypertension (PHT) is the most severe complication of liver cirrhosis. An increase in portal pressure can originate from a rise in portal blood flow, an increase in vascular resistance, or a combination of both.^[24] Increasing evidence also suggests that activated HSCs play an important role to intrahepatic haemodynamic changes in cirrhosis.^[13g] In a cirrhotic liver, portal hypertension can lead to bleeding—a life threatening complication and ultimately the cause of death in about one-third of patients.^[28]

It is well known that the protein endothelin (ET-1), which is markedly overexpressed within the cirrhotic liver, particularly in activated stellate cells constricts blood vessels plays a key role in the development of portal hypertension.^[29] The vasoconstrictive effects of ET-1 may be inhibited by

the introduction of vasodilators such as nitric oxide (NO) to relax the sinusoidal vasculature. Nitric oxide is endogenously produced from L-arginine by different forms of NO synthase (NOSs). After liver injury, intrahepatic NO is reduced due to the dysfunction of NO synthase.^[30] Thus, an attractive therapeutic option is the delivery of NO under specific conditions to overcome the endogenous underproduction of NO. Unfortunately, to date, the clinical utility of NO donors has been severely limited because of problems with both stability and specificity. For example, nonspecific NO donors, e.g., sodium nitroprusside and glyceryl trinitrate, cause vasodilation throughout the body, leading to highly undesirable effects on systemic haemodynamics. It is evident that NO donors reduce portal hypertension in animals models.^[24] The key challenge is the development of an NO donor that selectively targets the liver. In the present study, we demonstrated that vitamin A conjugated NO nanoparticles stabilize the NO donor while targeting HSCs. In further work, we investigated the effect of NO loaded nanoparticles on ET-1 induced contraction using a collagen gel contraction assay. The results shown in **Figure 10** corresponding to the NO nanoparticle treatment of

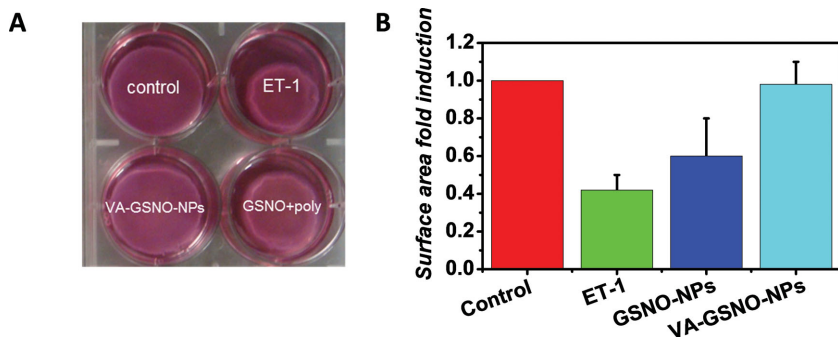


Figure 10. HSC collagen gel contraction assay. A) Picture of collagen gels; B) surface area fold induction versus different treatments. Data are mean \pm SD at least three experiments.

HSCs clearly indicate a reduced contractile response to ET-1. With vitamin A decoration on the nanoparticles plus ET-1, the accumulation of NO nanoparticles is significantly higher and the degree of gel contraction was lowest as indicated by

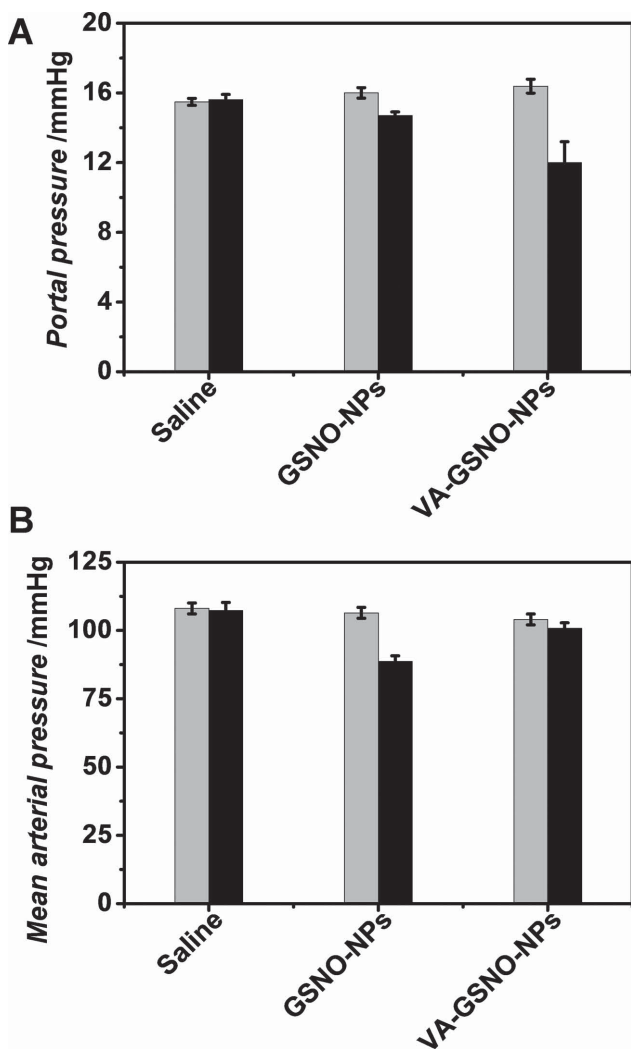


Figure 11. A) Portal pressure and B) mean arterial pressure versus different treatments (grey rectangle corresponds to control experiments). Note: Results are means \pm SD of four independent experiments performed.

the unchanging surface area, consistent with a decrease in α -SMA expression. Similar results were obtained using LX-2, a human HSC line (data not shown).

2.8. Portal and Arterial Pressure in a Rat Model of Cirrhosis

BDL rats were treated with vitamin A conjugated NO-nanoparticles, NO-nanoparticles (free vitamin A, as a control), and with saline solution (as a control). Portal pressure in BDL rats

treated with vitamin A conjugated NO nanoparticles was decreased by about 25% (\approx 12 mm Hg) (**Figure 11A**), while in vitamin A free nanoparticles and saline solution does not change the portal pressure. It has been reported that a reduction in portal pressure by 20% (15 mm Hg to about 12 mm Hg) significantly reduces the incidence of variceal haemorrhage.^[31,32] Ideally, a safe and effective treatment for portal hypertension in liver fibrosis would be liver-specific, reducing portal pressure without affecting the mean arterial pressure.^[33] To confirm that vitamin A conjugated NO nanoparticles have the potential to selectively deliver NO to the stellate cells in the liver, we have demonstrated that the administration of vitamin A conjugated NO nanoparticles significantly decreases the portal pressure in BDL rats, while having minimal influence on arterial pressure (Figure 11B). This result is another evidence that we are able to deliver specifically NO into the liver using targeted nanoparticles. As mentioned previously, direct measurement of NO in vivo is relatively difficult due to the inaccuracy measurement methods of NO in biologic media as recently reported by Hunter et al.^[27]

3. Conclusions

In this study, we report a new family of non-cytotoxic therapeutic nanoparticles, with efficacious targeting at the organ and cellular levels. We report the nanoparticle stabilization of NO donors and subsequent, nonsystemic, intracellular delivery of NO, down regulating the profibrogenic and contractile activity of hepatic stellate cells. These initial in vitro data are very promising, but in vitro experiments may not necessarily reflect in vivo. We have demonstrated a significant potential therapeutic benefit in mediating portal hypertension without any associated systemic side effects. This preliminary work shows significant promise in a health issue of widespread importance where there are few therapeutic options at present.

4. Experimental Section

Materials: OEGMA (Sigma-Aldrich) was passed through a column of basic alumina to remove inhibitor, prior to use. 2,2-azobisisobutyronitrile (AIBN) (Sigma-Aldrich) was crystallized from

methanol and stored at 0 °C before use. All other chemicals were purchased from Sigma-Aldrich, as supplied at the highest purity available. Retinol binding protein, Nycodenz and α -SMA mouse antibody were both purchased from Sigma-Aldrich (St. Louis, MO). Cy 7.5 NHS ester dye was purchased from Lumiprobe (USA). Pro-nase E, DNase I, and Collagenase B were purchased from Roche Applied Sciences (Indianapolis, IN). The BrdU ELISA kit was purchased from Roche Diagnostics (Castle Hills, NSW, Australia). The DMEM media was obtained from Invitrogen (Carlsbad, CA).

Equipment: ^1H NMR Analysis: All NMR spectra were recorded using a Bruker 300 MHz spectrometer. All chemical shifts are reported in ppm (δ) relative to tetramethylsilane, referenced to the chemical shifts of residual solvent resonances.

Gel Permeation Chromatography (GPC): GPC was used to determine the molecular weight and polydispersity index of the prepared polymers. The eluent used was *N,N*-dimethylacetamide [DMAc; 0.03% w/v LiBr, 0.05% w/v 2, 6-dibutyl-4-methylphenol (BHT)] at 50 °C (flow rate of 1 mL min $^{-1}$) on a Simadzu modular system comprised of a SIL-10AD autoinjector, a Polymer Laboratories 5.0 μL bead-size guard column (50 \times 7.8 mm) and four linear PL (Styragel) columns (10 5 , 10 4 , 10 3 , and 500 Å) and an RID-10A differential refractive-index detector. The GPC calibration was performed with narrow-polydispersity polystyrene standards ranging from 104 to 106 000 g/mol. A total of 50 μL of polymer solution (2 mg mL $^{-1}$ in DMAc) was injected for each analysis.

Attenuated Total Reflectance-Fourier Transform Infrared Spectroscopy (ATR-FTIR): ATR-FTIR measurements were performed on a Bruker IFS66\text{S} Fourier transform spectrometer by averaging 128 scans with a resolution of 4 cm $^{-1}$.

Dynamic Light Scattering (DLS): The average diameters and size distributions of the prepared micelles were measured using a Malvern Zetasizer Nano Series running DTS software (laser, 4 mW, λ = 633 nm; angle 173°). Samples were filtered to remove dust (microfilter 0.45 μm) prior to measurements.

UV-vis Spectroscopy: UV-vis measurements were recorded using a CARY 300 spectrophotometer (Bruker).

Raman Analysis: Raman spectra were acquired using a Raman-Station 400 coupled with Raman Micro 300 with an excitation wave length of 785 nm (PerkinElmer LAS GmbH). Raman spectra were recorded at room temperature over the spectral region from 200 to 1000 cm $^{-1}$ covering the S–S and C–S vibrational modes.

Transmission Electron Microscopy (TEM): TEM micrographs were obtained using a JEOL 1400 transmission electron microscope, operated at an acceleration voltage of 80 kV. The samples were prepared by casting micellar solutions (1 mg mL $^{-1}$) onto a formvar-coated copper grid. No staining was applied.

Mass Spectrometry Analysis: Electrospray-ionization mass spectrometry (ESI-MS) measurements were carried out using a Thermo Finnigan LCQ Deca ion trap mass spectrometer (Thermo Finnigan, San Jose, CA). The ESI-MS instrument was calibrated using caffeine, MRFA, and Ultramark 1621 (all from Aldrich) in the mass range 195–1822 Da. All spectra were acquired in positive ion mode over the mass to charge range, m/z , 100–2000 with a spray voltage of 5 kV, a capillary voltage of 44 V, and a capillary temperature of 275 °C. Nitrogen was used as the sheath gas and helium was used as auxiliary gas. The analysis sample (1 mg/ml) was prepared in a 60:40 v/v mixture of tetrahydrofuran (THF): methanol and an acetic acid concentration of 0.4×10^{-3} M. 56 Spectra were recorded in positive ion mode with an instrumental resolution of

0.1 Da. All reported molecular weights were calculated via the program package CS ChemDraw 12.0 and monoisotopic. The theoretical molecular weight to charge ratios (m/z , assuming $z+1$) were calculated using the exact molecular mass of the predominant isotope within the structure.

Methods: Synthesis of 4-Cyanopentanoic Acid Dithiobenzoate (CPADB): CPADB was prepared according to a previous publication.^[13a] A brief description was included in the Supporting Information.

Synthesis of 2-Vinyl-4,4-Dimethylazlactone (VDM): VDM was synthesized according to the method of Fontaine and co-workers.^[34] A brief description is given as follows:

Synthesis of *N*-Acryloyl-2-Methylalanine: A solution of 1.768 g (4.42×10^{-2} mol) of sodium hydroxide in 4.4 mL of water was cooled to 0 °C using an ice bath, are slowly added 2 g (1.94×10^{-2} mol) of 2-methylalanine and 2.0 mg (9.07×10^{-6} mol) of 2,6-di-*tert*-butyl-*p*-cresol. When the solution is homogeneous, 2 g (2.21×10^{-2} mol) of acryloyl chloride were added dropwise under stirring and keeping the temperature at 0 °C using an ice bath. After complete addition of acryloyl chloride, the stirring is continued for 3 h. To this solution was slowly added 2.3 mL of concentrated hydrochloric acid. During the addition a white solid is formed. The reaction solution was stirred for 30 min. The solid was filtered and was recrystallized from a mixture of ethanol and water (1/1 in volume). The white solid was filtered and dried under vacuum. Yield: 60%. mp 201–202 °C. ^1H NMR (300 MHz, DMSO d_6 , δ): 1.36 (s, C(CH $_3$) $_2$); 5.56 (dd, H_{trans} , $J_{Htrans-Hcis}$ = 2.1 Hz, $J_{Htrans-Hgem}$ = 10.1 Hz); 6.08 (dd, H_{cis} , $J_{Hcis-Htrans}$ = 2.1 Hz, $J_{Hcis-Hgem}$ = 17.1 Hz); 6.25 (dd, H_{gem} , $J_{Hgem-Htrans}$ = 10.1 Hz, $J_{Hgem-Hcis}$ = 17.1 Hz); 8.29 (s, NH–); 12.20 (s, COOH).

Synthesis of VDM: 0.4 g (2.54×10^{-3} mol) of *N*-acryloyl-2-methylalanine and 0.38 g (3.75×10^{-3} mol) of triethylamine were added to 10 mL of acetone. The resulting solution was cooled at 0 °C using an ice bath and 0.277 g (2.5×10^{-3} mol) of ethyl chloroformate was added dropwise. The solution was stirred for 3 h at 0 °C. The solution was then filtered and the white solid was washed with acetone. The filtrate was concentrated under vacuum and the filtrate residue was distilled under vacuum (bp 47 °C at 4 mm Hg) to give a colorless oil. Yield: 49%. ^1H NMR (300 MHz, CDCl $_3$, δ): 1.47 (s, C(CH $_3$) $_2$); 5.96 (dd, H_{trans} , $J_{Htrans-Hcis}$ = 2.0 Hz, $J_{Htrans-Hgem}$ = 9.9 Hz); 6.23 (dd, H_{cis} , $J_{Hcis-Htrans}$ = 2.0 Hz, $J_{Hcis-Hgem}$ = 17.6 Hz); 6.27 (dd, H_{gem} , $J_{Hgem-Htrans}$ = 9.9 Hz, $J_{Hgem-Hcis}$ = 17.6 Hz). ^{13}C NMR (300 MHz, CDCl $_3$, δ): 24.50 (C(CH $_3$) $_2$); 64.61 (C(CH $_3$) $_2$); 123.88 (CH $_2$ =CH); 128.81 (CH $_2$ =CH); 158.92 (C=N); 180.53 (C=O). FTIR, ν in cm $^{-1}$: 1820 (s, C=O); 1670 (w); 1651 (w); 1070 (s).

Synthesis of POEGMA MacroCTA: [OEG-MA] $_0$:[CPADB] $_0$:[AIBN] $_0$ = 100.0:1.0:0.1. OEG-MA $_{300}$ (2.3 g, 7.66×10^{-3} mol), CPADB (0.0214 g, 7.66×10^{-5} mol), AIBN (1.35 mg, 7.62×10^{-6} mol) and toluene (20 mL) were prepared in a round bottom flask (50 mL), equipped with a magnetic stirrer bar. The reaction mixture was degassed with nitrogen for 30 min. The degassed solution was immersed in a preheated oil bath at 70 °C for 17 h. The reaction was then placed in an ice bath for about 15 min to terminate polymerization and two aliquot were sampled for GPC and ^1H NMR analyses. The monomer conversion was determined by ^1H NMR analysis to be 67%. The reaction medium was precipitated in cold petroleum spirit (boiling range of 40–60 °C) and centrifuged (7000 rpm for 5 min). The precipitation and centrifugation steps were repeated three times to remove any traces of unreacted monomer and then

the reaction medium was dried in vacuum oven. POEGMA was analyzed by ^1H NMR and GPC. The molecular weight determined by GPC is 21 000 g/mol (M_n (theoretical) = 20 000 g/mol at 67% OEGMA conversion) and PDI = 1.12.

Synthesis of POEGMA-*b*-PVDM Block Copolymer: [POEGMA] $_0$:[VDM] $_0$:[AIBN] $_0$ = 1:144:0.25. POEGMA (M_n = 20 000 g/mol) (1.0 g, 5×10^{-5} mol), VDM (1.0 g, 7.3×10^{-3} mol) and AIBN (2 mg, 1.25×10^{-5} mol) were dissolved in 5 ml of toluene in a round bottom flask (10 mL), equipped with a magnetic stirrer bar. The reaction mixture was degassed with nitrogen for 45 min. The degassed solution was immersed in a preheated oil bath at 70 °C for 14 h. The reaction was then placed in an ice bath for about 15 min to terminate the polymerization and two aliquot were collected for GPC and ^1H NMR analyses. VDM conversion was determined by ^1H NMR analysis and is equal 60%. The reaction medium was precipitated in diethyl ether and centrifuged (7000 rpm for 5 min). The purification process was repeated three times and the reaction medium was dried in vacuum oven. The reaction was followed by ATR-FTIR to check the presence of azlactone functionality in the block copolymer (signal at 1820 cm^{-1}). The copolymers were analyzed by GPC, UV-vis, and ^1H NMR spectroscopy. The molecular weight (determined by GPC) is 33 000 g/mol (M_n (theoretical) = 32 000 g/mol at 60% VDM conversion) and PDI = 1.28.

Removal of Thiocarbonylthio End Group from the Polymeric Chain: The removal of RAFT end group was performed according to the method of Perrier et al.^[35] POEGMA-*b*-PVDM (1.0 g, 3.3×10^{-5} mol), AIBN (0.112 g, 6.9×10^{-4} mol), and toluene (6 mL) were added to a round bottom flask, equipped with a magnetic stirrer bar ([POEGMA-*b*-PVDM]:[AIBN] = 1:20). The reaction mixture was degassed with nitrogen for 20 min. The degassed solution was immersed in a preheated oil bath at 80 °C for 3 h. The reaction was then precipitated in diethyl ether and centrifuged. The purification process was repeated three times and the copolymer was dried in oven under vacuum. The samples were analyzed by ATR-FTIR to confirm the presence of azlactone groups after reaction at 1820 cm^{-1} . Aliquots were sampled for GPC, ^1H NMR and UV-vis analyses. UV-vis confirms the disappearance of RAFT agent.

Conjugation of Vitamin A to POEGMA-*b*-PVDM: POEGMA-*b*-PVDM (1.0 g, 2.86×10^{-5} mol), vitamin A (retinol, 14.0 mg, 4.95×10^{-5} mol), and DMSO (6 mL) were added to a round bottom flask, equipped with a magnetic stirrer bar ([POEGMA-*b*-PVDM]:[Retinol] = 1:2). The flask was placed in ice bath and degassed with nitrogen. 4-Dimethylaminopyridine (DMAP, 0.6 mg, 4.95×10^{-6} mol) and *N,N'*-Dicyclohexylcarbodiimide (DCC, 10 mg, 4.95×10^{-6} mol) were added. The reaction was carried out at room temperature overnight. The solid precipitate was removed by filtration, and the polymer was then precipitated in diethyl ether. The purification process was repeated three times and the copolymer was dried in oven under vacuum. The samples were analyzed by UV-vis to confirm the presence of vitamin A groups after reaction at 328 nm. Aliquots were sampled for GPC and ^1H NMR analyses. The molecular weight (determined by GPC) is 33 200 g/mol and PDI = 1.29.

Synthesis of GSNO: GSH (308 mg, 1×10^{-3} mol), HCl (0.1 mL, 32%), and water (3 mL) were prepared in a vial. The glass vial was put in an ice bath and covered with aluminum foil because GSNO is sensitive to light. Then, NaNO_2 (70 mg) was slowly poured into the bottle and the reaction was left for 30 min. The reaction was purified by precipitation twice in acetone: water mixture (4:1 v:v), twice in acetone, and finally, in diethyl ether. Then, GSNO

was dried in vacuum oven. Approximately 200 mg of pink solid is obtained (yield = 60%). Mass spectroscopy was performed to confirm the synthesis of GSNO. Signal at 347.15 Da (attributed to GSNO/ H^+) and at 369.13 (attributed GSNO/ Na^+) are observed.

Conjugation of GSNO to POEGMA-*b*-PVDM: 200 mg of POEGMA-*b*-PVDM (5.7×10^{-6} mol) was dissolved in DMF (500 μL). 163 mg of GSNO (4.86×10^{-4} mol) was also dissolved in DMSO (500 μL) in the presence of triethylamine (50 μL , 5×10^{-4} mol). GSNO solution was added to the block copolymer solution. Then, the reaction mixture was covered with aluminum foil and was left reacted at 30 °C for 5 h. The resulting reaction was characterized by ATR-FTIR, ^1H NMR, UV-vis.

Synthesis of NO-Nanoparticles: Equipped with a magnetic stirrer bar, water (5 mL) was added slowly the conjugated block copolymer with GSNO (100 mg) in DMSO (500 μL) under moderate stirring at room temperature to form NO nanoparticles, and then the mixture was dialyzed for 24 h. The water was changed every 3 h for 12 h. The NO-nanoparticles were then characterized by dynamic light scattering (DLS), transmission electron microscopy (TEM), and UV-vis spectrometry analysis.

Synthesis of NO-Nanoparticles with Vitamin A on the Surface: The procedure for the synthesis is similar to synthesis of NO nanoparticles, where POEGMA-*b*-PVDM block copolymer conjugated with vitamin A was used instead of POEGMA-*b*-PVDM block copolymer.

Synthesis of POEGMA-*b*-PVDM Nanoparticles labeled with Nile Red: Equipped with a magnetic stirrer bar, the block copolymer (100 mg) was dissolved in DMSO (1 mL) and Nile Red (5 mg) in DMSO (1 mL) was then added. Water (5 mL) was added dropwise at slow rate to form NO nanoparticles loaded with Nile Red, and then the mixture was dialyzed for 24 h against a 50/50 methanol and water mixture (by volume) and then water only. The water was changed every 3 h for 12 h. The NO-nanoparticles loaded with Nile Red were then characterized by dynamic light scattering (DLS), transmission electron microscopy (TEM), and UV-vis spectrometry analysis.

Synthesis of POEGMA-*b*-PVDM Nanoparticles (Labeled with Nile Red) with Vitamin A on the Surface: The procedure for the synthesis is similar to synthesis of POEGMA-*b*-PVDM nanoparticles labeled with Nile Red, where POEGMA-*b*-PVDM block copolymer conjugated with vitamin A was used instead of POEGMA-*b*-PVDM block copolymer.

Synthesis of POEGMA-*b*-PVDM Nanoparticles (Labeled with Cy7.5) with Vitamin A on the Surface: The procedure for the synthesis is similar to the synthesis of POEGMA-*b*-PVDM nanoparticles (labeled with Nile Red) with vitamin A on the surface, where a near-infrared fluorescent dye (Cy7.5) was used instead of Nile Red.

Cell Culture: The human hepatic cells LX-2 were grown in Dulbecco's Modified Eagle's Medium: Nutrient Mix F-12 (DMEM) supplemented with 10% (v/v) Fetal Calf Serum (FCS) in a ventilated tissue culture flask T-75. The cells were incubated at 37 °C in a 5% CO_2 humidified atmosphere and passaged every 2–3 days when monolayers at around 80% confluence were formed. Cell density was determined by counting the number of viable cells using a trypan blue dye (Sigma-Aldrich) exclusion test. For passaging and plating, cells were detached using 0.05% trypsin-EDTA (Invitrogen), stained using trypan blue dye, and loaded on the hemocytometer.

Cell Viability: The cytotoxicity of GSNO nanoparticles was tested in vitro by standard cell viability Alamar Blue Assay. The

assay is based on the ability of living cells to convert blue redox dye (resazurin) into bright red resorufin which can be read in a spectrophotometric reader.^[33] The intensity of the color is proportional to the cell viability. The LX-2 cells were seeded at 2000 cells/well for in 96 well tissue culture plates and incubated for 24 h. Cells were treated with fresh medium containing GSNO nanoparticles with concentration range from 10×10^{-6} to 1000×10^{-6} M (based on NO). At 72 h post-drug incubation, treatments were removed and fresh media was added (100 μ L) followed by the addition of Alamar Blue dye (20 μ L) to each well and the cells were incubated for 6 h and followed by spectrophotometric analysis. Cell viability was determined as a percentage of untreated control cells, and IC₅₀ values were calculated via regression analysis using Origi nanopartclesro 8 software.

Animals: Male Sprague-Dawley rats were obtained from the Animal Resources Centre (Perth, Australia). All animals were maintained under 12-h light/dark cycles with food and water ad libitum. For in vivo biodistribution experiment, BDL (bile duct ligation, 4 weeks) rat model was employed. All experimental protocols were approved by the Sydney West Area Health Service Animal Research Ethics Committee.

Isolation and Culture of Rat Hepatic Stellate Cells, Kupffer Cells and sinusoidal endothelial cells: Rat HSCs were isolated by two-step (collagenase B and pronase E) perfusion methods under ketamine and xylazine anaesthesia as reported previously.^[24] Briefly, rat liver was perfused through the portal vein using Ca⁺⁺- and Mg⁺⁺-free Gey's Balanced Salt Solution (GBSS, Sigma) and then sequentially with pronase E followed by collagenase B. The liver was excised, gently dispersed in GBSS containing 0.01% DNase I and the cell suspension filtered through a sterile nylon mesh and subjected to low-speed centrifugation. The resultant cell pellet was mixed with 30% Nycodenz to obtain an 11% final Nycodenz/cell suspension. After centrifugation at $1400 \times g$ for 20 min, HSCs were collected, resuspended in culture medium, and plated on 6 well plates with 10% FCS/DMEM at a density of 0.8×10^6 cells/well. Cell viability was assessed by trypan blue exclusion and was routinely over 95%. Purity was 95% as determined by morphology, vitamin A autofluorescence and desmin positivity. HSCs were maintained in 95% air, 5% CO₂ in DMEM with 10% FCS and 1% penicillin/Streptomycin. KCs and SECs were further obtained and purified by elutriation. KCs were identified by their ability to phagocytose latex beads; viability was >96% and purity >98%. The viability of SECs was >98% and purity at least 94% as determined by morphology (cobblestone appearance) and absence of latex bead phagocytosis. KCs were cultured in 10% FCS/DMEM/1% penicillin-streptomycin in 6 well plates. SECs were cultured in M199 with 20% FCS, 1% penicillin-streptomycin, insulin (20 mU mL⁻¹), heparin (10 U mL⁻¹), VEGF (5 ng mL⁻¹), and dexamethasone (10 μ mol L⁻¹). SEC culture wells were precoated with type I collagen (Nalge Nunc International, Rochester, NY). Hepatocytes were isolated according to the method as previously described by Lee and Farrell. Viability, assessed by trypan blue exclusion, and was always greater than 90%. Hepatocytes were plated onto plates coated with rat tail collagen 1 and cultured in Williams' E media supplemented with HEPES (18 mmol L⁻¹), NaHCO₃ (24 mmol/L), ascorbic acid (0.28 mmol L⁻¹), penicillin G (100 U mL⁻¹), and insulin (25 mU mL⁻¹).

Real Time Reverse Transcription Polymerase Chain Reaction: Total cellular RNA was prepared from HSCs using TRI[®] REAGENT (Molecular Research Center, INC, Cincinnati, OH). Complementary

DNA (cDNA) was synthesized from 1 μ g RNA using SuperScript III reverse transcriptase and 0.5 nmol of random primers (Invitrogen, Carlsbad, CA). Real-time quantitative reverse-transcription polymerase chain reaction (qRT-PCR) was performed using SYBR Green Platinum SYBR Green SuperMix (Invitrogen). The synthesized cDNA was amplified using the following sequence specific primers:

Collagen α 1(I)	5'-TTCACCTACAGCAGCTTG-3' (forward) and 5'-TCTTGGTGGTTTTGATTCGATGA-3' (reverse);
TGF β 1	5'-TCGACATGGAGCTGGTGA-3' (forward) and 5'-GAGCCTTAGTTGGACAGGATCTG-3' (reverse)
α SMA	5'-CGATAGAACACGGCATCATC-3' (forward) and 5'-CATCAGGCAGTTCGTAGCTC-3' (reverse)
TIMP1	5'-AAGGGCTACCAGAGCGATCA-3' (forward) and 5'-GGTATTGCCAGGTGCACAAAT-3' (reverse)
CTGF	5'-CGCCAACCGCAAGATTG-3' (forward) and 5'-ACACGGACCCACCGAAGAC-3' (reverse)

The relative amount of mRNA was calculated by reference to a calibration curve. The final result for each sample was normalized to the respective β actin value.

Uptake of GSNO Nanoparticles by Liver Cells Using Flow Cytometry: Primary rat HSCs, KCs, SECs, and hepatocytes ($\approx 10^5$ each cell type) were incubated with GSNO (500×10^{-6} M), VA-decorated nanoparticles-GSNO (10 μ L mL⁻¹-equivalent to 500×10^{-6} M GSNO), VA-nanoparticles-GSNO (in the presence of RBP) (10 μ L mL⁻¹-equivalent to 500×10^{-6} M GSNO) for various time courses (15, 30, 60, and 120 min). Fluorescence intensity was determined by flow cytometry. To avoid nonspecific uptakes by liver cells, we chose 30 min as optimal time point for the following experiments.

DAF-FM Detection of Nitric Oxide in LX-2 Cells: For this purpose, LX-2 cells (4000 cells/well) were plated into 4 well Lab Tek[™] chamber slides precoated with poly-D-lysine hydrobromide (Sigma-Aldrich) for 10 min. After 4 days, cells were loaded with the probe by replacing media with DMEM containing the 5×10^{-6} M DAF-FM DA and incubated at 37 °C for 20 min (Scheme S2, Supporting Information). The cells were then washed three times with media to remove excess probe and then incubated with fresh media for 15 min to complete de-esterification of the intracellular diacetates. The GSNO nanoparticles (250×10^{-6} M) were added to LX-2 cells loaded with DAF-FM for 6 h in the presence of ascorbic acid (5×10^{-3} M) for the more efficient NO release. Upon the completion of NO donor treatment, cells were then rinsed with PBS and fixed in 4% paraformaldehyde for 10 min at room temperature. Following fixation, cell plasma membrane was stained with Alexa Fluor 594 wheat germ agglutinin (5.0 μ g mL⁻¹) for 10 min at room temperature. When labelling is complete, the labelling solution was removed and cells were washed twice in PBS solution. The slides were then left to air dry briefly, prior to adding ProLong[®] Gold Antifade Reagent with DAPI mounting media and covering with a coverslip. The slide was stored in the dark overnight and then sealed with nail polish. Slides were stored at 4 °C until required for imaging using confocal laser scanning microscopy (CLSM). CLSM images of cells were captured using a confocal microscope (Zeiss LSM 780) with a 40 \times glycerol immersion objective (1.2 numerical apertures). Released nitric oxide upon reaction with DAF-FM, Alexa Fluor 594 wheat germ agglutinin, DAPI was detected at an

emission/excitation maxima of 495/515, 591/618, 350/461 nm, respectively. All the experiments were done in triplicate.

HSC Proliferation: Cell proliferation was analyzed using a BrdU-based enzyme-linked immunosorbent assay (Roche Diagnostics) according to the manufacturer's instructions. Rat primary HSCs at day 6 and LX-2 cell line were treated with GSNO (500×10^{-6} M), VA-nanoparticles-GSNO ($10 \mu\text{L mL}^{-1}$ -equivalent to GSNO 500×10^{-6} M), VA-nanoparticles-GSNO (in the presence of RBP) ($10 \mu\text{L mL}^{-1}$ -equivalent to GSNO, 500×10^{-6} M) for 30 min and then media were washed off and cells were washed three times with PBS, fresh media were replaced for 24 h culture. Subsequently, cells were labeled with BrdU for 2 h at 37 °C. Cells were then fixed and incubated with a peroxidase-conjugated anti-BrdU antibody for 90 min at room temperature. After adding the peroxidase substrate 3,3',5,5'-tetramethylbenzidine, BrdU incorporation was determined by measuring optical densities at 450 nm (background 620 nm).

HSC Migration: Cell migration was assessed by the wound scratch assay. HSCs at day 6 and LX-2 cell line (90% confluence) cultured in 12 well plates were used. Using a sterile 200 μL pipette tip, three separate wounds were generated through the cell monolayer. The floating cells were rinsed with PBS and the media replaced with nanoparticles-GSNO (500×10^{-6} M), VA-nanoparticles-GSNO ($10 \mu\text{L mL}^{-1}$ -equivalent to GSNO 500×10^{-6} M), VA-nanoparticles-GSNO (in the presence of RBP) ($10 \mu\text{L mL}^{-1}$ -equivalent to GSNO 500×10^{-6} M) for 30 min. Media were then washed off and cells were washed three times with PBS, fresh media were replaced. The scratch area was photographed immediately and 6 h after scratching and cell migration into the scratch area calculated as the area covered by cells in the percentage of the initial scratch area.

HSC Apoptosis: Annexin-V/PI labeling was used to detect HSC apoptosis. Briefly, trypsinized HSCs and LX-2 cells were washed twice in PBS, stained with annexin-V (10 μL) and PI (5 μL) for 10 min, and the apoptotic rate quantified by FACS Calibur flow cytometry (Becton Dickinson Inc.) at 488 nm. More than 1×10^4 cells were detected, and the results were analyzed with FlowJo software (TreeStar, USA). The population of apoptotic cells was identified as annexin V+/PI-. The percentage of apoptotic cells was calculated according to total annexin V+/PI- divided by total cells.

HSC Contraction Determined by Collagen Gel Assay: HSCs at 6 days (0.5×10^6 cells/well/6 well plate) were treated with nanoparticles-GSNO (500×10^{-6} M), VA-nanoparticles-GSNO ($10 \mu\text{L mL}^{-1}$ -equivalent to GSNO 500×10^{-6} M), VA-nanoparticles-GSNO (in the presence of RBP) ($10 \mu\text{L mL}^{-1}$ -equivalent to GSNO 500×10^{-6} M) for 30 min and then media were washed off and cells were washed three times with PBS. Subsequently, HSCs were trypsinized and transferred on to hydrated collagen gels prepared using rat tail collagen I (pH 7.4). After detaching matrices, the medium was supplemented in the various wells with ET-1 (10 nmol L^{-1}) for 6 h. Cell-mediated contraction is measured by determining the surface area of matrices.

Organ Biodistribution of VA-Nanoparticles-GSNO in Rat by Spectrometry: Normal and BDL rat were sacrificed by carbon dioxide asphyxiation after VA-nanoparticles-GSNO labeled with Nile Red was injected via tail vein for 2 h. The major organs (liver, kidney, eye, heart, spleen, brain, intestines, and lung) were removed and then were subjected to a homogenization procedure. The appropriate volume of PBS (0.5 mL mg^{-1} of tissue) was added

to each tissue prior to homogenization to an even consistency. The fluorescence intensity of these organs was determined by spectrometry at 460 nm.

Organ Biodistribution of VA-Nanoparticles-GSNO in Rat Using Small Animal Imager: Normal rat (≈ 100 g) was anesthetized and VA-nanoparticles-GSNO was injected via tail vein (0.2 mL) in a normal pressure. Images were observed at various time points of post-injection (0, 15, 30, 60 min, 2, 4, 20, 48, 72, 96, and 120 h). All fluorescence images were acquired with one second exposure ($f/\text{stop} = 4$).

Acute Anti-Portal Hypertensive Effects of VA-Decorated Nanoparticles-GSNO in BDL Rat: BDL rat (≈ 200 g) was used. Hemodynamic measurements were performed under isoflurane anesthesia. Portal pressure and mean arterial pressure were detected before and 15 min after injection of saline (vehicle, 1 mL), nanoparticles-GSNO (168 mg dissolved in 1 mL saline-equivalent to 500×10^{-6} M in rat blood), VA-nanoparticles-GSNO (0.2 mL nanoparticle dissolved in 1 mL saline).

Statistical Analysis: The results are expressed as mean \pm SD. Comparisons between two groups were analyzed using the Student t test. A 2-sided p value <0.05 was used to connote significance. For the comparison of more than two groups, we used two-way ANOVA.

Supporting Information

Supporting Information is available from the Wiley Online Library or from the author.

Acknowledgments

H.T.T.D. and Z.D. contributed equally to this work. The authors thank Dr. Christopher Brownlee for the valuable discussion on the flow cytometry data. The authors also thank the Nuclear Magnetic Resonance facility, Biological Resources Imaging Laboratory, Biomedical Imaging facility, and the Electron Microscope Unit at the Mark Wainwright Analytical Centre for helpful discussions and advice on the design of the experimental setup. C.B. is thankful for his fellowship from Australian Research Council (APD-ARC and Future Fellowship (ARC-FT 120100096)). This work was in part supported by Grant Nos. 1004595 and 632630 from the National Health and Medical Research Council (NHRMC) of Australia and the Robert W. Storr Bequest to the Sydney Medical Foundation, University of Sydney.

- [1] a) A. Burnett, C. Lowenstein, D. Bredt, T. Chang, S. Snyder, *Science* **1992**, 257, 401; b) J. R. Lancaster, *Science* **2004**, 304, 1905; c) S. Snyder, *Science* **1992**, 257, 494.
- [2] S. B. Williams, J. A. Cusco, M.-A. Roddy, M. T. Johnstone, M. A. Creager, *J. Am. Coll. Cardiol.* **1996**, 27, 567.
- [3] a) G. Aram, J. J. Potter, X. Liu, M. S. Torbenson, E. Mezey, *Hepatology* **2008**, 47, 2051; b) D. C. Rockey, V. Shah, *Hepatology* **2004**, 39, 250.
- [4] R. O. Cannon, *Clin. Chem.* **1998**, 44, 1809.

- [5] K. J. Smith, H. Lassmann, *Lancet Neurol.* **2002**, *1*, 232.
- [6] S. Mocellin, V. Bronte, D. Nitti, *Med. Res. Rev.* **2007**, *27*, 317.
- [7] a) R. Bataller, xF, D. A. Brenner, *J. Clin. Invest.* **2005**, *115*, 209; b) J. Li, T. R. Billiar, *Am. J. Phys. – Gastrointest. Liver Phys.* **1999**, *276*, G1069.
- [8] S. L. Friedman, *Gastroenterology* **2008**, *134*, 1655.
- [9] D. Y. Zhang, S. L. Friedman, *Hepatology* **2012**, *56*, 769.
- [10] a) R. Vercelino, I. Crespo, G. P. Souza, M. Cuevas, M. Oliveira, N. Marroni, J. González-Gallego, M. Tuñón, *J. Mol. Med.* **2010**, *88*, 401; b) O. Lukivskaya, E. Patsenker, R. Lis, V. U. Buko, *Eur. J. Clin. Invest.* **2008**, *38*, 317.
- [11] G. Ali, S. Mohsin, M. Khan, G. Nasir, S. Shams, S. Khan, S. Riazuddin, *J. Transl. Med.* **2012**, *10*, 75.
- [12] a) T. B. Cai, P. G. Wang, A. A. Holder, *Nitric Oxide Donors: For Pharmaceutical and Biological Applications*, Wiley-VCH, Weinheim **2005**; b) T. Yamamoto, R. J. Bing, *Proc. Soc. Exp. Biol. Med.* **2000**, *225*, 200.
- [13] a) H. T. T. Duong, Z. M. Kamarudin, R. B. Erlich, Y. Li, M. W. Jones, M. Kavallaris, C. Boyer, T. P. Davis, *Chem. Commun.* **2013**, *49*, 4190; b) M. C. Jen, M. C. Serrano, R. van Lith, G. A. Ameer, *Adv. Funct. Mater.* **2012**, *22*, 239; c) S. Duan, S. Cai, Q. Yang, M. L. Forrest, *Biomaterials* **2012**, *33*, 3243; d) A. J. Kutner, A. J. Friedman, *Wiley Interdiscip. Rev.: Nanomed. Nanobiotechnol.* **2013**, *5*, 502; e) P. Cabrales, G. Han, P. Nacharaju, A. J. Friedman, J. M. Friedman, *Am. J. Physiol.: Heart Circ. Physiol.* **2011**, *300*; f) P. Cabrales, *Virulence* **2011**, *2*, 185; g) P. Cabrales, G. M. Zanini, D. Meays, J. A. Frangos, L. J. M. Carvalho, *J. Infect. Dis.* **2011**, *203*, 1454; h) P. Cabrales, G. Han, C. Roche, P. Nacharaju, A. J. Friedman, J. M. Friedman, *Free Radical Biol. Med.* **2010**, *49*, 530.
- [14] a) P. Sauvant, M. Cansell, C. Atgié, *J. Physiol. Biochem.* **2011**, *67*, 487; b) Y.-S. Lee, W.-I. Jeong, *J. Gastroenterol. Hepatol.* **2012**, *27*, 75.
- [15] Y. Sato, K. Murase, J. Kato, M. Kobune, T. Sato, Y. Kawano, R. Takimoto, K. Takada, K. Miyanishi, T. Matsunaga, T. Takayama, Y. Niitsu, *Nat. Biotech.* **2008**, *26*, 431.
- [16] a) C. Boyer, V. Bulmus, T. P. Davis, V. Admiral, J. Liu, S. Perrier, *Chem. Rev.* **2009**, *109*, 5402; b) G. Moad, E. Rizzardo, S. H. Thang, *Aust. J. Chem.* **2005**, *58*, 379.
- [17] J.-W. Park, G. Means, *Arch. Pharm. Res.* **1989**, *12*, 257.
- [18] G. M. Walsh, D. Leane, N. Moran, T. E. Keyes, R. J. Forster, D. Kenny, S. O'Neill, *Biochemistry* **2007**, *46*, 6429.
- [19] C. Alric, I. Miladi, D. Kryza, J. Taleb, F. Lux, R. Bazzi, C. Billotey, M. Janier, P. Perriat, S. Roux, O. Tillement, *Nanoscale* **2013**, *5*, 5930.
- [20] A. Albanese, P. S. Tang, W. C. W. Chan, *Ann. Rev. Biomed. Eng.* **2012**, *14*, 1.
- [21] A. Cardenas, *Am. J. Gastroenterol.* **2005**, *100*, 460.
- [22] C. Whiting, A. Castillo, M. Z. Haque, D. S. A. Majid, *Am. J. Phys.: Renal Phys.* **2013**, *305*, F1031.
- [23] a) S. M. Moghimi, A. C. Hunter, J. C. Murray, *Pharm. Rev.* **2001**, *53*, 283; b) R. Bansal, E. Post, J. H. Proost, A. de Jager-Krikken, K. Poelstra, J. Prakash, *J. Controlled Release* **2011**, *154*, 233.
- [24] Z. X. Dong, L. Su, J. Brymora, C. Bird, Q. Xie, J. George, J. H. Wang, *World J. Gastroenterol.* **2013**, *19*, 4475.
- [25] D. A. Langer, A. Das, D. Semela, N. Kang-Decker, H. Hendrickson, S. F. Bronk, Z. S. Katusic, G. J. Gores, V. H. Shah, *Hepatology* **2008**, *47*, 1983.
- [26] E. Planchet, W. M. Kaiser, *J. Exp. Bot.* **2006**, *57*, 3043.
- [27] R. A. Hunter, W. L. Storm, P. N. Coneski, M. H. Schoenfisch, *Anal. Chem.* **2013**, *85*, 1957.
- [28] R. de Franchis, M. Primignani, *Clin. Liver Dis.* **2001**, *5*, 645.
- [29] S. Tièche, A. De Gottardi, A. Kappeler, S. Shaw, H. Sägesser, A. Zimmermann, J. Reichen, *J. Hepatol.* **2001**, *34*, 38.
- [30] C. Edwards, H. Q. Feng, C. Reynolds, L. Mao, D. C. Rockey, *Am. J. Phys.: Gastrointest. Liver Phys.* **2008**, *294*, G1311.
- [31] T. Y. E. Liaw, N. K. Salam, M. J. McKay, A. M. Cunningham, D. E. Hibbs, M. Kavallaris, *Mol. Cancer Ther.* **2008**, *7*, 3150.
- [32] G. Garcia-Tsao, A. J. Sanyal, N. D. Grace, W. Carey, *Hepatology* **2007**, *46*, 922.
- [33] a) D. C. Rockey, *Clin. Liver Dis.* **2006**, *10*, 459; b) H. Reynaert, M. G. Thompson, T. Thomas, A. Geerts, *Gut.* **2002**, *50*, 571.
- [34] M. E. Levere, H. T. Ho, S. Pascual, L. Fontaine, *Polym. Chem.* **2011**, *2*, 2878.
- [35] S. Perrier, P. Takolpuckdee, C. A. Mars, *Macromolecules* **2005**, *38*, 2033.

Received: September 25, 2014
Revised: November 19, 2014
Published online: